Article

Evolution of Microstructure, Properties, and Fracture Behavior with Annealing Temperature in Complex Phase Steel with High Formability

Xiaohong Chu [1,2], Feng Zhou [1,2], Lei Liu [1,2], Xiaolong Xu [1,2], Xiaoyue Ma [1,2], Weinan Li [1,2] and Zhengzhi Zhao [1,2,*]

[1] Collaborative Innovation Center of Steel Technology, University of Science and Technology Beijing, Beijing 100083, China; d202110602@xs.ustb.edu.cn (X.C.); d202110603@xs.ustb.edu.cn (F.Z.); d202210629@xs.ustb.edu.cn (L.L.); m202211286@xs.ustb.edu.cn (X.X.); m202221344@xs.ustb.edu.cn (X.M.); m202221342@xs.ustb.edu.cn (W.L.)

[2] Beijing Engineering Technology Research Center of Special Steel for Traffic and Energy, University of Science and Technology Beijing, Beijing 100083, China

* Correspondence: zhaozhzhi@ustb.edu.cn; Tel.: +86-10-6233-2617

Abstract: In recent years, with the continuous improvement in the requirements for automobile steel formability, complex phase steel with high formability (CH steel) has been widely used. In the present study, the microstructure of CH steel was regulated using the actual production process as a basis and annealing temperature as a variable, and the effects of annealing temperature on the microstructure, properties, and fracture behavior of CH steel were analyzed. As the annealing temperature increases, the ferrite content decreases from 36.3% to 0, the martensite content decreases from 49.3% to 8.8%, the bainite content increases from 11.9% to 87.1%, and the retained austenite content first increases and then decreases within the range of 2.5~5.1%. Consequently, the tensile strength shows a decreasing trend, the yield strength first decreases and then increases, and the total elongation and the hole expansion ratio first increase and then decrease. The deformation coordination of each phase gradually becomes better, and the voids and cracks in the tensile and hole expansion samples expand along the ferrite and martensite or martensite/austenite (M/A) island interface, transforming into the bainitic ferrite and martensite or M/A islands. The test steel's best tensile and hole expansion properties occur at annealing temperatures of 940 °C.

Keywords: complex phase steel with high formability; annealing temperature; microstructure; properties; fracture behavior

1. Introduction

With the continuous development of the automobile industry, automobile production has been increasing, bringing about environmental pollution problems that have gradually attracted attention. At present, automobile lightweight engineering is currently a more effective solution [1,2]. At the same time, as the concept of integrating automobile structural parts gradually enters the public eye and requirements for automobile esthetics continue to increase, the shapes of automobile structural parts become increasingly complex. In summary, it is worth paying attention to improving the formability while also improving the strength of automotive steel.

The microstructure of complex phase (CP) steel is a small amount of martensite (M), retained austenite (RA), or pearlite distributed on the ferrite (F) or bainite (B) matrix [3,4]. Compared with high-strength steels of the same grade, such as dual phase (DP) steel, transformation-induced plasticity (TRIP) steel, quenching and partitioning (Q-P) steel, and medium manganese steel, CP steel has higher yield strength, stretch–flangeability, and bending properties [5–7]. It can be used to manufacture various parts that require high local formability, such as door sills, door anti-collision bars, seat slide rails, chassis

suspension parts, and other safety parts, so it has been widely used. Based on this, the concept of complex phase steel with high formability (CH) was proposed in the standard VDA 239-100 and revised in the new steel grade. Introducing a small amount of retained austenite into CP steel causes the TRIP effect, and the elongation of CH steel is higher than that of CP steel with the same tensile strength [8]. The microstructure of CH steel consists of ferrite, martensite, bainite, and retained austenite. The development of CH steel is achieved by adopting the ideas of low carbon and microalloy strengthening combined with reasonable processes.

There are few studies on CH steel. However, with the trend of improving strength and achieving lightweight automobile parts, CH steel with its wide application is urgently needed to achieve high strength and formability. In existing studies, the effects of composition, isothermal temperature, and precursors on the microstructure and properties of CH steel have been explored [9,10]. Cr retards the bainite transformation and refines the grain size of CH steel, and Cr promotes the precipitation of (Nb, Ti)C in the high-temperature austenite region. The strength has an increasing tendency and the total elongation has a decreasing tendency with the increase in isothermal temperature [9]. The lower recrystallization rate promotes bainite transformation and increases the dislocation strengthening, grain refinement strengthening, and precipitation strengthening of CH steel [10]. It is well known that the annealing temperature has a significant impact on the proportion of each phase [11]. However, as an important heat treatment parameter, the impact of annealing temperature on the microstructure and properties of CH steel has not been analyzed. Among similar steels, such as TRIP steel and Q-P steel, no quantitative analysis of the effect of annealing temperature on the microstructure has been carried out, and no analysis has been carried out to comprehensively analyze the mechanical properties, hole expansion properties, and fracture mechanism of this steel [12,13].

Herein, annealing temperature was used as a variable to prepare CH steel with different proportions of each phase. The effect of annealing temperature on the microstructure, mechanical properties, and hole expansion properties of CH steel was analyzed, and the fracture behavior was expounded, which is essential for optimizing the microstructure and properties of CH steel and offers a theoretical basis for CH steel production.

2. Materials and Methods

2.1. Materials and Heat Treatment

The chemical composition of the test steel is Fe-0.17C-1.60(Si+Al)-2.65Mn-0.30Cr-0.20Mo-0.08(Nb+Ti) (wt.%) and the quenching device dilatometer Bähr DIL805A (Thermoanalyse GmbH, Hüllhorst, Germany) was used to test the austenite transformation start temperature (A_{c1}), which was 704 °C, and the austenite transformation end temperature (A_{c3}), which was 972 °C [9,10]. After smelting, forging, and hot rolling, a hot-rolled sheet with a thickness of 4 mm was obtained after five rolling passes. The heating furnace temperature, the hot rolling start temperature, the final rolling temperature, and the laminar cooling temperature were 1200 °C, 1150 °C, 890 °C, and 550 °C, and the furnace was kept at 550 °C for 1 h to simulate coiling. Finally, after pickling and cold rolling, a cold-rolled sheet with a thickness of 1.7 mm was obtained for subsequent heat treatment experiments. The heat treatment was carried out on the continuous annealing simulator CCT-AY-II (Ulvac-Riko INC, Tokyo, Japan). The cold-rolled sheet was heated to the annealing temperature ranging from 800 °C to 990 °C for 90 s at a heating rate of 10 °C/s. It was quickly cooled to 380 °C for 600 s at a rate of 45 °C/s, then cooled at 10 °C/s to room temperature. The continuous annealing process route is shown in Figure 1. Hereafter, test steels containing different microstructure were obtained, which are referred to as 800, 850, 900, 940, and 990, respectively.
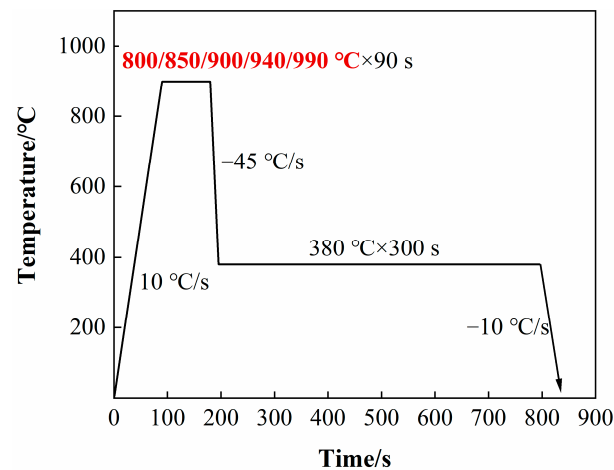
Figure 1. Schematic diagram of continuous annealing process route.

2.2. Microstructure Characterization and Property Testing

Microstructure, void, and crack characterization were achieved using scanning electron microscopy (SEM, Gemini SEM 500, Oberkochen, Germany). The SEM samples were ground, polished, and etched with 4% nitric acid. An electron backscatter diffraction (EBSD) measurement (20 kV, step size: 0.08 μm) was performed with a detector (Symmetry S2, Oxord Instruments, Abingdon, UK) mounted on the SEM. EBSD data were processed by Aztec software 2.1.2. EBSD samples were tested after electrolytic polishing in an electrolyte solution of 10 vol.% perchloric acid and 90 vol.% ethanol. The current was controlled at about 1 A, the voltage was set to 13 V, electrolytic polishing was performed at room temperature, and the polishing time was about 30 s. The fine microstructure and precipitation were observed with a transmission electron microscope (TEM, JEM 2100, Tokyo, Japan). The samples ground to 60 μm were twin-jet polished and thinned in a solution of 5 vol.% perchlorate alcohol at −30 °C in preparation for TEM testing. Using a Bruker D8-Advance diffractometer (Karlsruhe, Germany) and Cu Kα radiation (wavelength λ = 0.1542 nm), X-ray diffraction (XRD) examinations were used to measure the volume fraction (V_γ) and carbon content (C_γ) of RA. The samples were scanned at a rate of 2°/min within a 2θ range from 38° to 94°. The V_γ was calculated using Formula (1) [10,14]:

$$V_\gamma = 1.4 I_\gamma / (I_\alpha + 1.4 I_\gamma) \tag{1}$$

where I_γ and I_α are the average integral intensity of the $(200)_\gamma$, $(220)_\gamma$, and $(311)_\gamma$ austenite peaks and that of the $(200)_\alpha$ and $(211)_\alpha$ ferrite peaks. The C_γ was calculated using Formulas (2) and (3) [15,16]:

$$C_\gamma = (a_\gamma - 3.547)/0.046 \tag{2}$$

$$a_\gamma = \frac{\lambda \sqrt{h^2 + k^2 + l^2}}{2 \sin\theta_{hkl}} \tag{3}$$

where a_γ is the austenite's lattice parameter, which is calculated as an average using the $(200)_\gamma$, $(220)_\gamma$, and $(311)_\gamma$ austenite peaks; (hkl) and θ_{hkl} are the three Miller indices of a plane and the Bragg angle.

The quenching device dilatometer Bähr DIL805A was used to simulate the continuous annealing process for quantitative analysis of bainite, and the cooling medium was nitrogen. The ferrite content during the intercritical annealing process was measured by being cooled to room temperature at a cooling rate of 45 °C/s directly after the intercritical annealing. The room-temperature tensile test was performed using the tensile testing machine MTSE45.305 (MTS Systems Corporation, Eden Prairie, MN, USA) with a tensile speed of 1 mm/min. Tensile samples with a gauge length of 25 mm and a gauge width of 6 mm were cut along the

rolling direction. The punching and hole expansion processes were carried out on a plate formability testing machine BUP600 (Zwick, Ulm, Germany), and the hole expansion ratio (HER) was used to measure the stretch–flangeability. The punched hole with a diameter of 10 mm was used in the hole expansion test with a 60° conical punch until a crack through the thickness of the plate appeared on the edge of the hole. The driving speed of the conical punch was 0.2 mm/s. Three samples were used for tensile and hole expansion tests, and the average value was calculated.

3. Results and Discussion

3.1. Effect of Annealing Temperature on Microstructure of CH Steel

The microstructure of the cold-rolled sheet is granular bainite (GB) deformed along the rolling direction, and the microstructure of the annealed steel is GB, martensite, retained austenite, and/or polygonal ferrite, as shown in Figure 2. Granular bainite is small islands composed of M/A islands dispersed on a bainite ferrite matrix with a high density of dislocations. As the annealing temperature increases, the ferrite content and martensite content gradually decrease, while the bainite content gradually increases. The morphology of M/A islands in bainite gradually transforms from blocky to filmy and is distributed in a certain orientation. The blocky martensite gradually transforms from an interconnected network form to be distributed at the prior austenite grain boundaries, and the size is larger in 990 steel than in 940 steel.
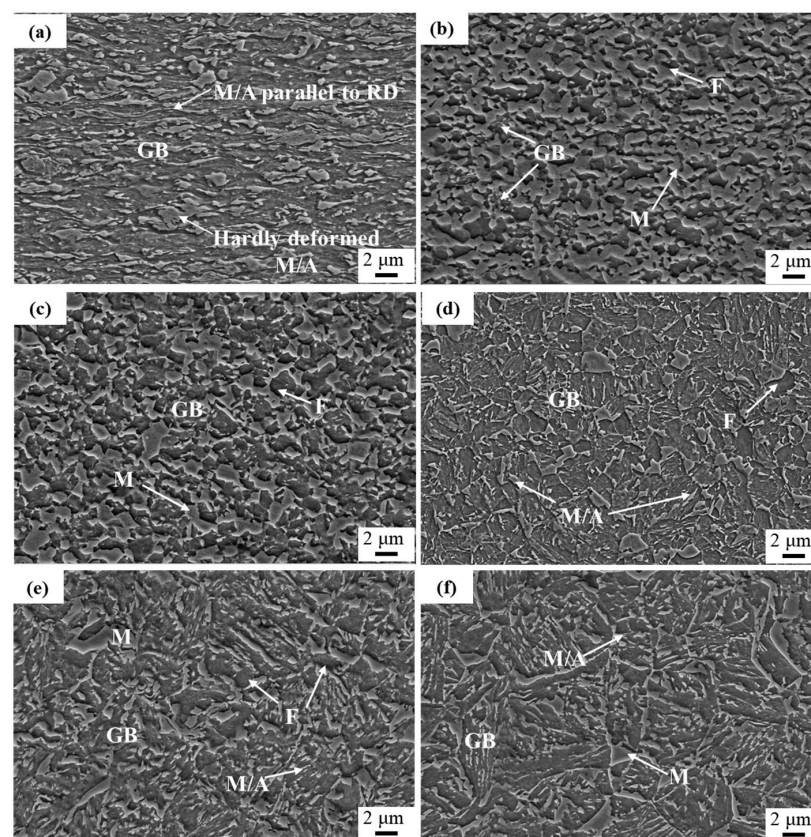

Figure 2. SEM microstructure analysis. (**a**) The cold-rolled sheet; (**b**) 800; (**c**) 850; (**d**) 900; (**e**) 940; (**f**) 990.

In order to quantify each phase, XRD was used to test the volume fraction of retained austenite and its carbon content, and dilatometry was used to test the bainite content. The bainite contents were approximately estimated by the change in the linear thermal expansion coefficient (LTEC) due to the LTEC of each phase in the steel being different, and we also used this method in previous studies [9,10,17]. The XRD test results, dilatometry

changes in the isothermal bainite zone, and the quantitative analysis results are shown in Figures 3 and 4. As the annealing temperature increases, the ferrite content decreases from 36.3% to 0, the martensite content decreases from 49.3% to 8.8%, and the bainite content increases from 11.9% to 87.1% and becomes an important component phase. The RA content first increases and then decreases, which is related to the content of untransformed austenite and its stability [18,19]. With the increase in the annealing temperature, the austenite and bainite contents increase, leading to a higher carbon content in untransformed austenite diffused from bainite isothermally at 380 °C. Thus, the stability of RA improves, and the austenite content retained after quenching increases. However, as the annealing temperature increases further, the bainite transformation increases, the untransformed austenite decreases, and even though the untransformed austenite is rich in carbon, the RA content at room temperature is less, such as that in 990 steel. When the annealing temperature is 940 °C, the retained austenite content is the highest, at 5.1%.
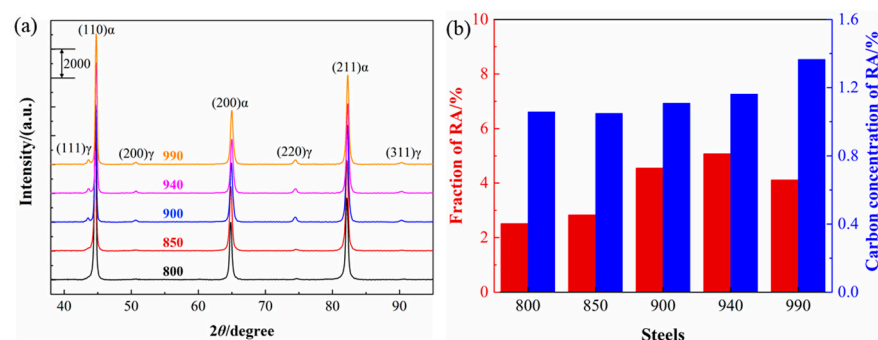

Figure 3. XRD test results. (**a**) XRD patterns; (**b**) retained austenite and its carbon content.
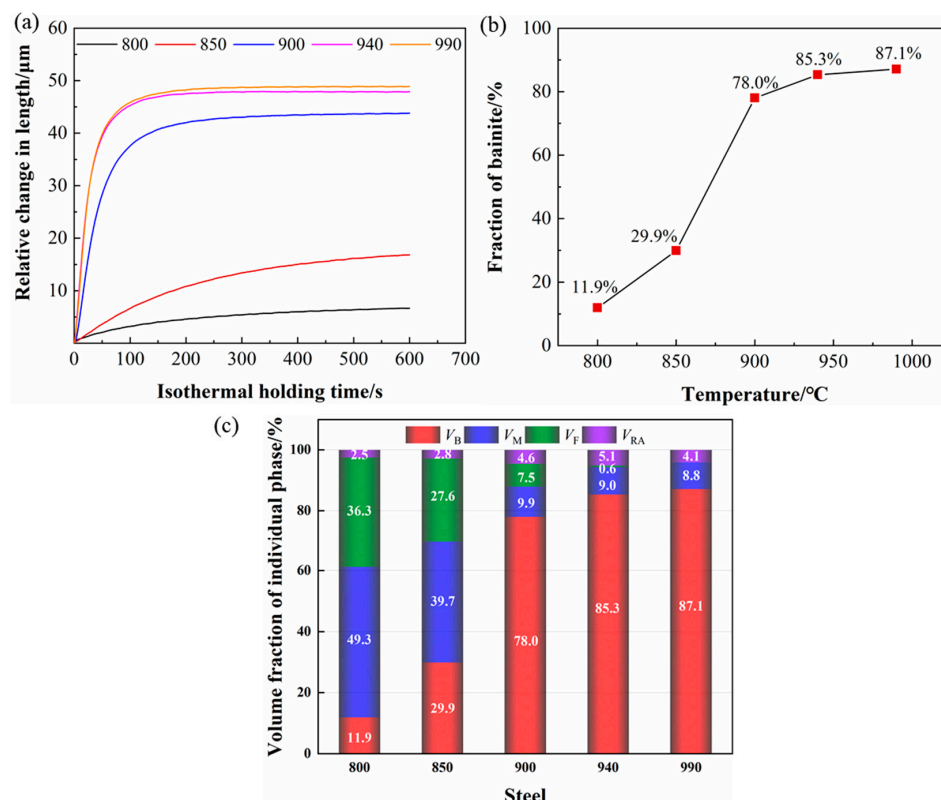

Figure 4. Quantitative analysis. (**a**) Relative changes in length with isothermal holding time; (**b**) fraction of bainite at different annealing temperatures; (**c**) volume fraction of individual phases.

The microstructure was further analyzed accurately, and the EBSD test and TEM test results are shown in Figures 5 and 6. Compared with the cold-rolled sheet, the annealed sheets have no obvious orientation and the average kernel average misorient (KAM) value is significantly reduced. It is obvious that as the annealing temperature increases, the average grain size gradually increases, from 0.77 μm to 1.20 μm, as shown in Figure 5s,t. When the annealing temperature is 800 °C, the KAM value is larger. The larger KAM values are mainly distributed in martensite or M/A islands with lower band contrast (BC) values, while the KAM value inside the ferrite is lower. As the annealing temperature increases, the average KAM value gradually decreases and becomes uniform, mainly distributed in the internal laths of bainite. Due to the reduced martensite content, the average BC value of the maps decreases significantly. For the retained austenite, it gradually changes from being distributed in blocky forms at the grain boundaries during low-temperature annealing to filmy forms within the bainite laths during high-temperature annealing.
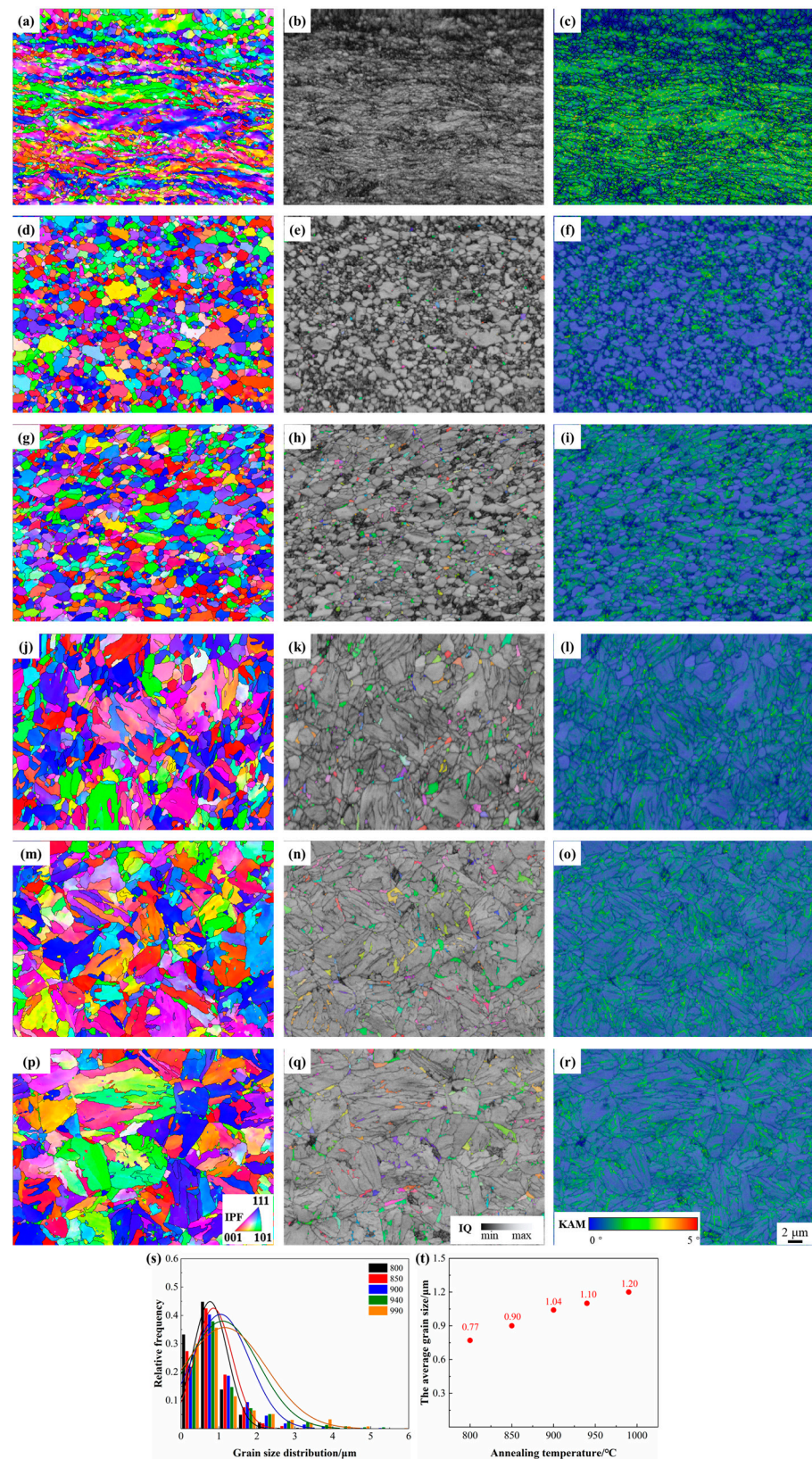
When the annealing temperature is 800 °C, polygonal ferrite and blocky martensite exist in smaller sizes. It is worth noting that there is obvious dislocation accumulation at the interface between ferrite and martensite, as shown in Figure 6b. In addition, since a small amount of Nb and Ti microalloying elements are added to the test steel, nano-scale (Nb, Ti)C is evenly distributed, which can play an effective role in precipitation strengthening [10,20]. When the annealing temperature is 940 °C, bainite laths are obvious and distributed with high dislocation density, and M/A islands are distributed at the grain boundaries. The retained austenite is not only distributed in the form of a film between the bainite laths, but is also distributed inside bainite ferrite. The latter is generally identified as M/A islands in a SEM map.

3.2. Effect of Annealing Temperature on Properties of CH Steel

The tensile properties and hole expansion properties of the steels tested at annealing temperatures ranging from 800 °C to 990 °C are shown in Table 1 and Figure 7. For the test steels with different annealing temperatures, the yield strength ranges from 658 MPa to 873 MPa, the tensile strength ranges from 1110 MPa to 1410 MPa, the total elongation ranges from 11.7% to 15.0%, and the HER ranges from 5.3% to 28.8%. As the annealing temperature increases, the tensile strength shows a decreasing trend, and the yield strength first decreases and then increases. The total elongation and the hole expansion ratio first increase and then decrease, reaching their maximum values at 940 °C. Taken together, when the annealing temperature is 940 °C, the comprehensive mechanical properties of the test steel are better, with a product of strength and elongation (PSE) of 16.7 GPa% and an HER of 28.8%.

Table 1. Properties at different annealing temperatures.

Steel	Tensile Strength/MPa	Yield Strength/MPa	Total Elongation/%	PSE/(GPa%)	HER/%
800	1410	749	12.3	17.3	5.3
850	1229	658	14.2	17.5	10.1
900	1120	836	14.2	15.9	20.8
940	1110	867	15.0	16.7	28.8
990	1131	873	11.7	13.2	24.0

Figure 5. EBSD test results of (**a**–**c**) cold-rolled sheet, (**d**–**f**) 800, (**g**–**i**) 850, (**j**–**l**) 900, (**m**–**o**) 940, and (**p**–**r**) 990. (**a**,**d**,**g**,**j**,**m**,**p**) Inverse pole figure (IPF) map, (**b**,**e**,**h**,**k**,**n**,**q**) distribution of RA (IPF map of RA is superimposed on BC map), (**c**,**f**,**i**,**l**,**o**,**r**) BC and KAM map, (**s**) grain size distribution of annealed steels, and (**t**) average grain size changes with annealing temperature.

Figure 6. TEM test results for (**a**–**c**) 800 and (**d**–**f**) 940. (**a**,**d**) Overall morphology of 800 and 940; (**b**) dislocation accumulation at F/M interface; (**c**) precipitation; (**e**) retained austenite in bainite laths; (**f**) filmy M/A islands inside bainite.
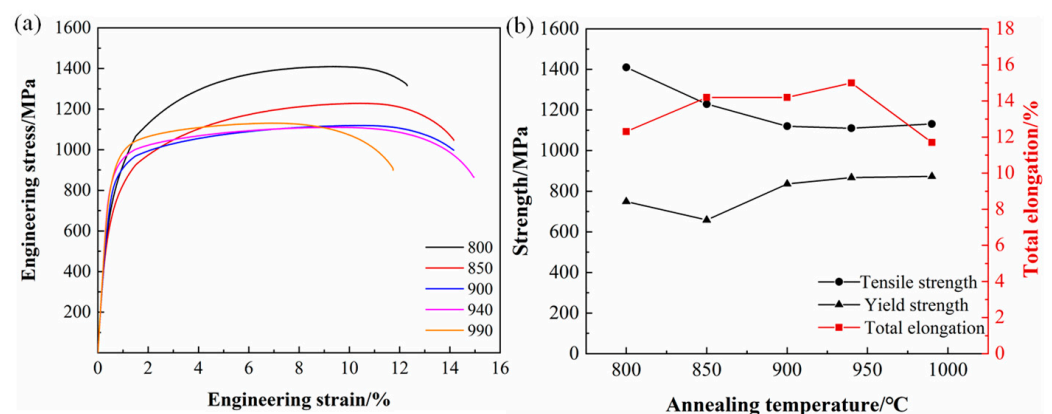

Figure 7. Mechanical properties. (**a**) The engineering stress–strain curves; (**b**) changes in the mechanical properties with annealing temperature.

All of the test steels show continuous yielding behavior. The initial decrease in the yield strength and tensile strength can be attributed to the reduction in martensite content. The increased bainite content leads to an increase in the yield strength. When the annealing temperature approaches A_{C3}, the soft phase ferrite and martensite decrease, bainite increases, and the tensile strength changes a little. The initial increase in elongation can be attributed to the rise in bainite and retained austenite content and the decrease in martensite content [21,22]. The higher content of retained austenite leads to a further increase in the elongation of 940. When the annealing temperature is 990 °C, the grain size increases to 1.20 μm, and the plasticity required for larger grain destruction decreases [23]. In addition, the soft phase ferrite and retained austenite contents decrease, and the elongation decreases.

It is generally believed that the size and content of the hard phase, the strength difference between the soft and hard phases, and the RA content are the keys to determining the HER [24–27]. In this study, the RA content in CH steel is small. The cracks will not be caused by the huge difference in hardness between the high-carbon martensite transformed by a large amount of retained austenite after punching and the low-carbon martensite and the adversely affected formability. The larger martensite content of 800, 850, and 900 results in lower hole expansion ratios. As the annealing temperature increases, the bainite content gradually increases, alleviating the deformation difference caused by the severe strength difference between the soft and hard phases. The HER of 940 steel reaches the maximum.

As the annealing temperature further increases, the grain size of 990 increases significantly, and the large-sized blocky martensite distributed in the prior austenitic grain boundaries leads to a reduction in the HER.

3.3. Fracture Behavior Analysis

To further analyze CH steel's damage and fracture mechanism, the tensile and hole expansion fracture samples were analyzed, as shown in Figures 8–10. The macromorphology and microstructure of the tensile fracture section are shown in Figure 8. The macromorphology of the fracture is shown in Figure 8a,d,g,j,m, which are all ductile fractures. As the annealing temperature increases, the porosities (black arrow) show a downward trend. The fracture shape of 800 is relatively flat, most of the fracture surface is 90° to the tensile direction, and the plastic deformation is not obvious. The fracture shapes of 850, 900, 940, and 990 are similar to a cup shape, with apparent necking. The fracture surfaces are 45° to the tensile direction, and the plastic deformation is obvious. The microstructure near the fracture and the area 10 mm away from the fracture is shown in Figure 8b,c,e,f,h,i,k,l,n,o. The microstructure is elongated along the direction of stress, and the locations of voids and cracks are mainly distributed (1) near the interface between M or M/A islands and the matrix (red arrow); (2) in M or M/A islands themselves (blue arrow) [12]. Both situations exist in the 800 and 850 samples. The plastic incompatibility between ferrite and blocky martensite in the low-temperature annealed microstructure leads to stress concentration and dislocation accumulation [28], which leads to cracking and so a large crack along the F/M interface and passing through M is still found in the area around the fracture and 10 mm away from the fracture, as shown in Figure 8c,f. Research shows that when the martensite content is higher than 20%, martensite is prone to fracture [29,30]. As the annealing temperature increases, the bainite content increases, the deformation of each phase becomes more coordinated, and the deformation along the tensile direction becomes more apparent [31]. The number of voids and cracks are reduced, and their locations are mainly near the interface between M or M/A islands and bainitic ferrite (BF), especially at the interface between BF and larger M forms. For bainite formed at lower isothermal temperatures, M/A islands exhibit twice the hardness and more considerable shear stress compared to bainitic ferrite [32]. During deformation, there is a difference in the plastic deformation between the M/A island and the BF. Then, dislocations accumulate at the interface between the M/A island and the BF, resulting in a plastic strain concentration area, which is not conducive to improving the plasticity and toughness.

Figure 9 shows the macromorphology and the central fracture zone microstructure of the tensile fracture surface. As the annealing temperature increases, the fracture characteristics gradually change from quasi-cleavage and dimple mixed type to dimple type, mainly due to the reduction in martensite content and the improvement in the interconnected network morphology of martensite [33]. A previous study has shown that quasi-cleavage fracture does not affect plasticity as seriously as cleavage fracture does [34]. As the grain size increases from 0.77 μm to 1.20 μm, the dimple size shows an increasing trend. The 900's fracture surface has double-sized dimples. Some large-sized dimples with large depths indicate that the aggregation of dimples has experienced intense plastic deformation, which is conducive to an increase in elongation, making 900 have a higher elongation under conditions with more blocky martensite content [35]. In the 940 sample, the dimple size is uniformly smaller, the depth is larger, and the performance is the best. For the 990 sample, the dimple size is uneven, the dimple depth is shallow, and the plasticity is poor [36]. In addition, the third-principal strain at fracture ε_{3f} (the true thickness strain at the fracture) was calculated, which can be used to measure local formability and is proportional to the HER [37]. As the fracture toughness increases along the thickness direction, the initiation of cracks at the hole's edge is delayed, thereby delaying the expansion along the thickness direction and increasing the HER [38].
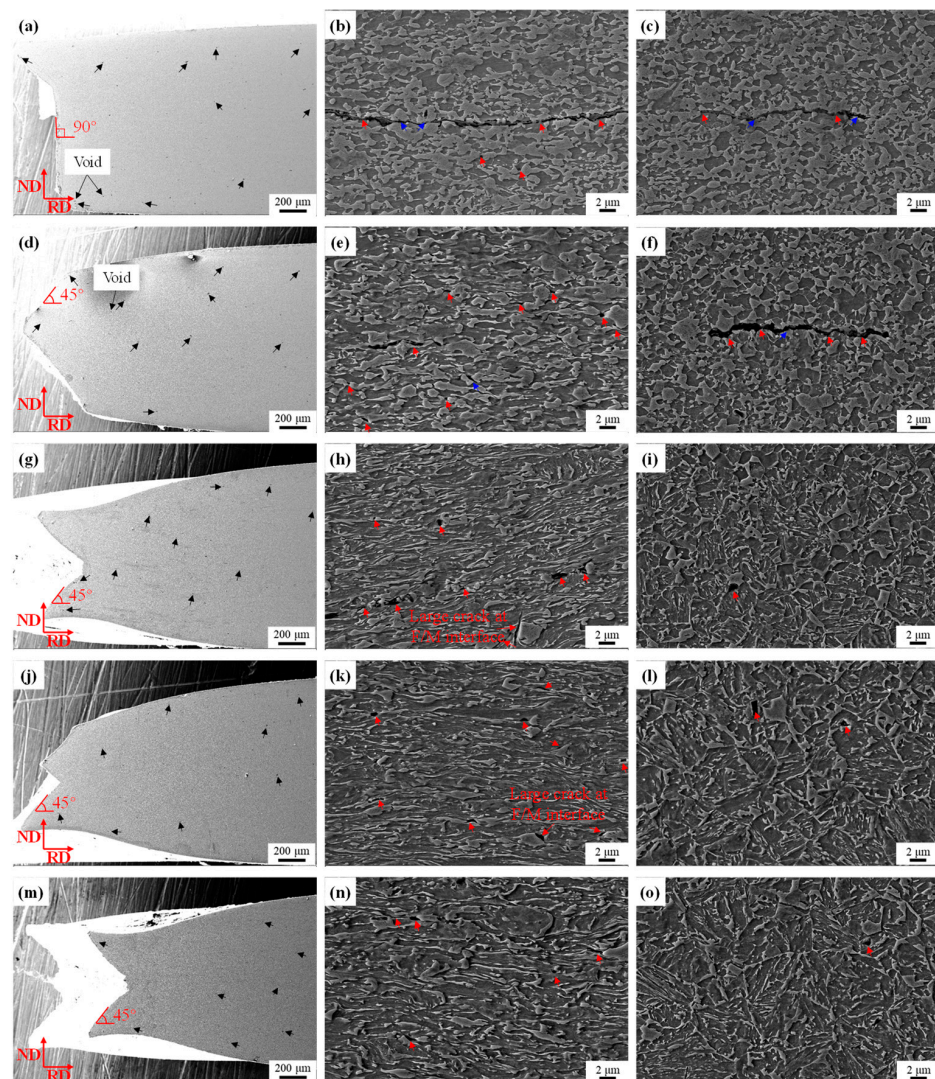
Figure 8. Tensile fracture morphology. (**a**,**d**,**g**,**j**,**m**) Macromorphology, (**b**,**e**,**h**,**k**,**n**) microstructure near the fracture, and (**c**,**f**,**i**,**l**,**o**) microstructure of the area 10 mm away from the fracture of 800, 850, 900, 940, and 990, respectively.

Additionally, as seen in Figure 10, the macromorphology and microstructure of the edge of the hole expansion samples were analyzed. The grains rotate along the shear direction, and voids and cracks occur along the shear direction. The higher the hole expansion ratio, the closer the deformation direction to 90°, as shown by the white dotted line. When the annealing temperature is lower, the ferrite content of 800 steel is higher. After the hole expansion test, the ferrite is connected to form a band, and the cracks expand along the interface between the ferrite and the M or M/A island and go through the large size M. The same is true for the fracture of the 850 sample. As the annealing temperature increases, the voids and cracks in 940 mainly occur at the BF and M/A island interfaces. Figure 10f,g show the crack growth of 900 and 990, which mainly extends along the BF and M/A island interfaces and bypasses or ends up with large-sized martensite [39]. The initiation and expansion of cracks in materials follow the principle of minimum energy. Dislocation accumulation or soft and hard phase interfaces are the locations with the lowest energy consumption, so voids and cracks can easily occur. In short, for high-strength CH steel composed of multiple phases, the key to improving performance is to rationally adjust the chemical composition and heat treatment process to optimize the ratio of soft and hard phases.
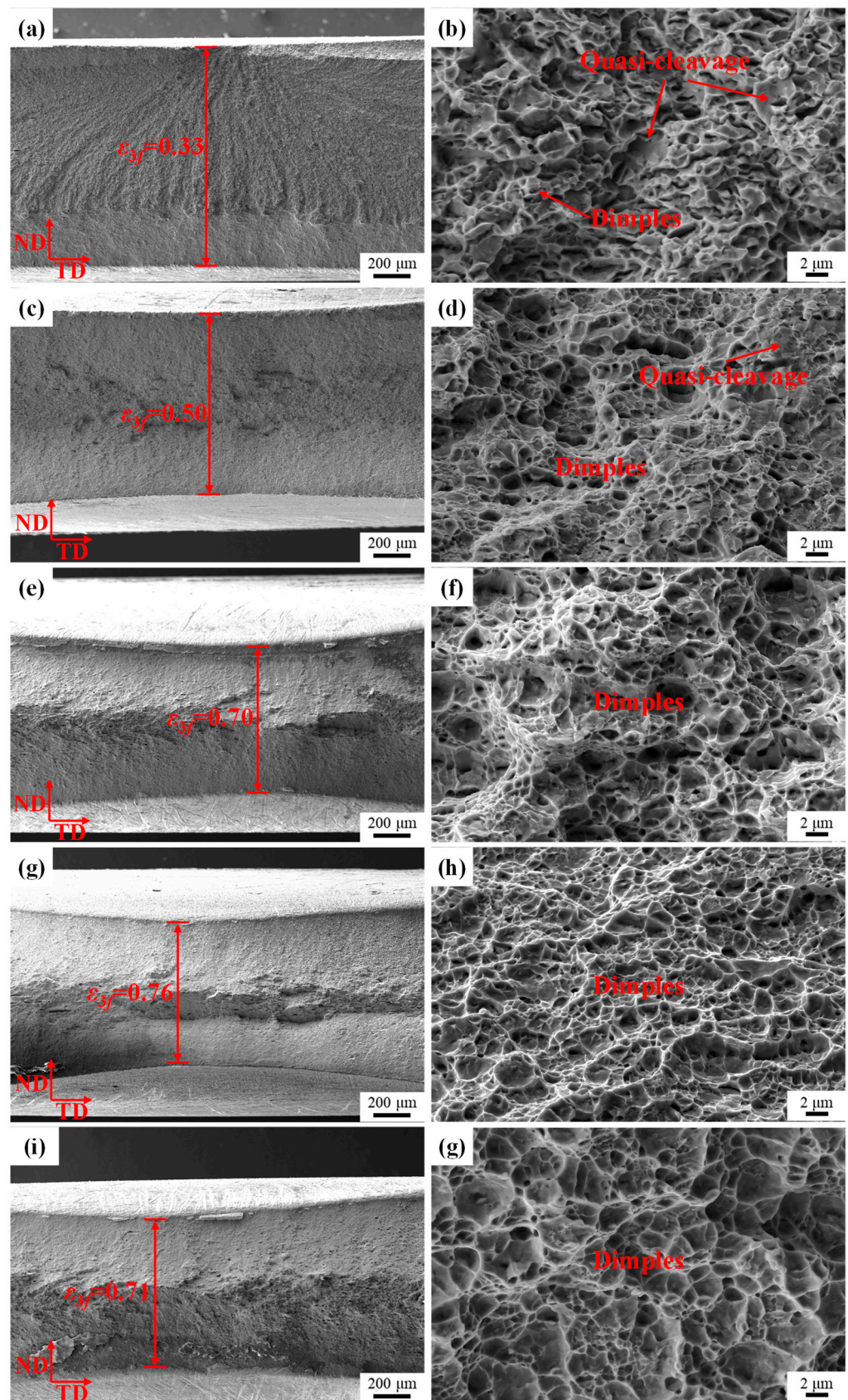
Figure 9. The macromorphology and the central fracture zone microstructure of the tensile fracture surface of (**a**,**b**) 800, (**c**,**d**) 850, (**e**,**f**) 900, (**g**,**h**) 940, and (**i**,**g**) 990.
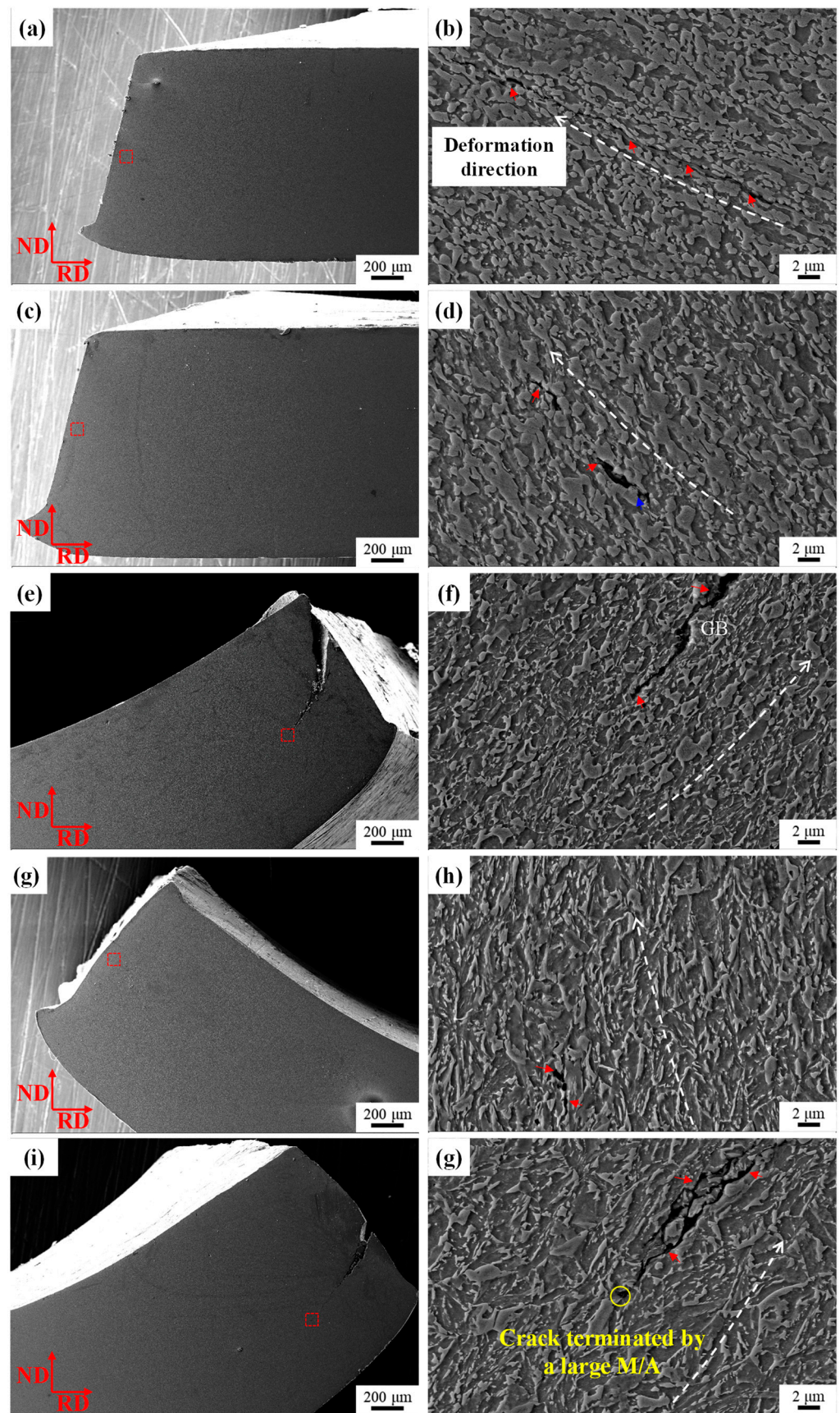
Figure 10. The macromorphology and microstructure of the edge of the hole expansion samples (the micromorphology is in the red dotted box of the macromorphology). (**a**,**b**) 800, (**c**,**d**) 850, (**e**,**f**) 900, (**g**,**h**) 940, and (**i**,**g**) 990.

4. Conclusions

The evolution of the microstructure and properties of CH steel with annealing temperature were analyzed by SEM, EBSD, XRD, TEM, and property testing machines. The main conclusions are summarized as follows:

(1) CH steel with different proportions of each phase is prepared by taking the annealing temperature as a variable. As the annealing temperature increases, the grain size gradually increases, the ferrite and martensite contents gradually decrease, the bainite content rises from 11.9% to 87.1%, becoming a vital component phase, and the retained austenite content shows a trend of increasing first and then decreasing.

(2) As the annealing temperature increases, the tensile strength shows a decreasing trend, the yield strength first decreases and then increases, and the total elongation and the HER first increase and then decrease. When the annealing temperature is 940 °C, the comprehensive properties of the test steel are the best. The present steel not only creates outstanding CH steel but also offers a theoretical basis for CH steel production.

(3) Tensile fractures are all ductile fractures. As the annealing temperature increases, the porosities show a decreasing trend. The positions of voids and cracks are mainly near the interface between M or M/A islands and BF, and M or M/A islands no longer have fractures; the fracture characteristics gradually change from quasi-cleavage and dimple mixed type to dimple type, and the true thickness strain at the fracture is directly proportional to the HER. The grains of the hole expansion samples rotate along the shear direction. The voids and cracks propagate along the interface between ferrite and martensite or the M/A islands transform into the interface between BF and martensite or M/A islands with increased annealing temperature.

References

1. Kuziak, R.; Kawalla, R.; Waengler, S. Advanced High Strength Steels for Automotive Industry. *Arch. Civ. Mech. Eng.* **2008**, *8*, 103–117. [CrossRef]
2. Trzepieciński, T.; Najm, S.M. Current Trends in Metallic Materials for Body Panels and Structural Members Used in the Automotive Industry. *Materials* **2024**, *17*, 590. [CrossRef]
3. Correia Lima, R.d.M.; dos Santos Fernandes Tolomelli, F.T.; Clarke, A.J.; Clarke, K.D.; Spadotto, J.C.; Rizzo Assuncao, F.C. Microstructural Characterization of a 1100 MPa Complex-Phase Steel. *J. Mater. Res. Technol.* **2022**, *17*, 184–191.
4. Szeliga, D.; Chang, Y.; Madej, L.; Bzowski, K.; Perzyński, K.; Haase, C.; Bleck, W.; Pietrzyk, M. Correlating the Microstructural Heterogeneity with Local Formability of Cold-Rolled Dual-Phase and Complex-Phase Steels Through Hardness Gradients. *Steel Res. Int.* **2022**, *93*, 2200130. [CrossRef]
5. Shen, F.; Wang, H.; Liu, Z.; Liu, W.; Könemann, M.; Yuan, G.; Wang, G.; Münstermann, S.; Lian, J. Local Formability of Medium-Mn Steel. *J. Mater. Process. Technol.* **2022**, *299*, 117368. [CrossRef]
6. Li, Z.; Chang, Y.; Rong, J.; Min, J.; Lian, J. Edge Fracture of the First and Third-Generation High-Strength Steels: DP1000 and QP1000. *IOP Conf. Ser. Mater. Sci. Eng.* **2023**, *1284*, 12021. [CrossRef]
7. Fonstein, N.; Jun, H.-J.; Huang, G.; Sriram, S.; Yan, B. Effect of Bainite on Mechanical Properties of Multiphase Ferrite-Bainite-Martensite Steels. *Mater. Sci. Technol.* **2011**, *1*, 333–341.
8. Sugimoto, K.; Nakano, K.; Song, S.-M.; Kashima, T. Retained Austenite Characteristics and Stretch-Flangeability of High-Strength Low-Alloy TRIP Type Bainitic Sheet Steels. *ISIJ Int.* **2002**, *42*, 450–455. [CrossRef]

9. Chu, X.; Gao, P.; Chen, W.; Li, F.; Kang, T.; Zhao, Y.; Yin, X.; Zhao, Z. Effect of Cr and Isothermal Holding Temperature on Microstructure and Properties of Complex Phase Steel with High Formability (CH Steel). *J. Iron Steel Res. Int.* **2023**, *30*, 328–337. [CrossRef]

10. Chu, X.; Zhao, Y.; Yang, Y.; Zhou, F.; Liu, L.; Zhao, Z. Effect of Recrystallization on Bainite Transformation and Mechanical Properties of Complex Phase Steel with High Formability (CH Steel). *J. Mater. Res. Technol.* **2023**, *26*, 7674–7693. [CrossRef]

11. Mohanty, R.R.; Girina, O.A.; Fonstein, N.M. Effect of Heating Rate on the Austenite Formation in Low-Carbon High-Strength Steels Annealed in the Intercritical Region. *Metall. Mater. Trans. A* **2011**, *42*, 3680–3690. [CrossRef]

12. Wang, Y.; Xu, Y.; Wang, X.; Zhang, J.; Peng, F.; Gu, X.; Wang, Y.; Zhao, W. Improving the Stretch Flangeability of Ultra-High Strength TRIP-Assisted Steels by Introducing Banded Structure. *Mater. Sci. Eng. A* **2022**, *852*, 143722. [CrossRef]

13. Wang, X.; Liu, L.; Liu, R.D.; Huang, M.X. Benefits of Intercritical Annealing in Quenching and Partitioning Steel. *Metall. Mater. Trans. A* **2018**, *49*, 1460–1464. [CrossRef]

14. Sugimoto, K.; Usui, N.; Kobayashi, M.; Hashimoto, S. Effects of Volume Fraction and Stability of Retained Austenite on Ductility of TRIP-Aided Dual-Phase Steels. *ISIJ Int.* **1992**, *32*, 1311–1318. [CrossRef]

15. Sugimoto, K.; Iida, T.; Sakaguchi, J.; Kashima, T. Retained Austenite Characteristics and Tensile Properties in a TRIP Type Bainitic Sheet Steel. *ISIJ Int.* **2000**, *40*, 902–908. [CrossRef]

16. Yan, S.; Liu, X.; Liu, W.J.; Lan, H.; Wu, H. Microstructural Evolution and Mechanical Properties of Low-Carbon Steel Treated by a Two-Step Quenching and Partitioning Process. *Mater. Sci. Eng. A* **2015**, *640*, 137–146. [CrossRef]

17. Gao, G.; Zhang, H.; Gui, X.; Luo, P.; Tan, Z.; Bai, B. Enhanced Ductility and Toughness in an Ultrahigh-Strength Mn–Si–Cr–C Steel: The Great Potential of Ultrafine Filmy Retained Austenite. *Acta Mater.* **2014**, *76*, 425–433. [CrossRef]

18. Lu, J.; Wang, S.; Yu, H.; Wu, G.; Gao, J.; Wu, H.; Zhao, H.; Zhang, C.; Mao, X. Structure-Property Relationship in Vanadium Micro-Alloyed TRIP Steel Subjected to the Isothermal Bainite Transformation Process. *Mater. Sci. Eng. A* **2023**, *878*, 145208. [CrossRef]

19. Lu, J.; Yu, H.; Duan, X.; Song, C. Investigation of Microstructural Evolution and Bainite Transformation Kinetics of Multi-Phase Steel. *Mater. Sci. Eng. A* **2020**, *774*, 138868. [CrossRef]

20. Song, C.; Wang, H.; Sun, Z.; Yu, H. Analysis of Precipitation Characteristics of TiC at Different Quenching and Partitioning Temperatures and Its Effect on the Mechanical Properties. *Mater. Sci. Eng. A* **2021**, *824*, 141868. [CrossRef]

21. Seo, E.J.; Cho, L.; Estrin, Y.; De Cooman, B.C. Microstructure-Mechanical Properties Relationships for Quenching and Partitioning (Q&P) Processed Steel. *Acta Mater.* **2016**, *113*, 124–139.

22. Xiong, X.C.; Chen, B.; Huang, M.X.; Wang, J.F.; Wang, L. The Effect of Morphology on the Stability of Retained Austenite in a Quenched and Partitioned Steel. *Scr. Mater.* **2013**, *68*, 321–324. [CrossRef]

23. Calcagnotto, M.; Ponge, D.; Raabe, D. Effect of Grain Refinement to 1 μm on Strength and Toughness of Dual-Phase Steels. *Mater. Sci. Eng. A* **2010**, *527*, 7832–7840. [CrossRef]

24. Karelova, A.; Krempaszky, C.; Werner, E.; Tsipouridis, P.; Hebesberger, T.; Pichler, A. Hole Expansion of Dual-Phase and Complex-Phase AHS Steels—Effect of Edge Conditions. *Steel Res. Int.* **2009**, *80*, 71–77.

25. Paul, S.K. A Critical Review on Hole Expansion Ratio. *Materialia* **2020**, *9*, 100566. [CrossRef]

26. Song, E.; Lee, G.-H.; Jeon, H.; Park, B.J.; Lee, J.-G.; Kim, J.-Y. Stretch-Flangeability Correlated with Hardness Distribution and Strain-Hardenability of Constituent Phases in Dual- and Complex-Phase Steels. *Mater. Sci. Eng. Struct. Mater. Prop. Microstruct. Process.* **2021**, *817*, 141353. [CrossRef]

27. Kim, J.H.; Lee, S.W.; Lee, K.; Kim, J.-K.; Suh, D.-W. Effect of Prior Austenite Grain Size on Hole Expansion Ratio of Quenching and Partitioning Processed Medium-Mn Steel. *JOM* **2019**, *71*, 1366–1374. [CrossRef]

28. Erdogan, M. The Effect of New Ferrite Content on the Tensile Fracture Behaviour of Dual Phase Steels. *J. Mater. Sci.* **2002**, *37*, 3623–3630. [CrossRef]

29. Lai, Q.; Bouaziz, O.; Gouné, M.; Brassart, L.; Verdier, M.; Parry, G.; Perlade, A.; Bréchet, Y.; Pardoen, T. Damage and Fracture of Dual-Phase Steels: Influence of Martensite Volume Fraction. *Mater. Sci. Eng. A* **2015**, *646*, 322–331. [CrossRef]

30. Szewczyk, A.F.; Gurland, J. A Study of the Deformation and Fracture of a Dual-Phase Steel. *Metall. Trans. A* **1982**, *13*, 1821–1826. [CrossRef]

31. Tan, X.; Ponge, D.; Lu, W.; Xu, Y.; He, H.; Yan, J.; Wu, D.; Raabe, D. Joint Investigation of Strain Partitioning and Chemical Partitioning in Ferrite-Containing TRIP-Assisted Steels. *Acta Mater.* **2020**, *186*, 374–388. [CrossRef]

32. Lan, L.; Yu, M.; Qiu, C. On the Local Mechanical Properties of Isothermally Transformed Bainite in Low Carbon Steel. *Mater. Sci. Eng. A* **2019**, *742*, 442–450. [CrossRef]

33. Huang, J.X.; Liu, Y.; Xu, T.; Chen, X.F.; Lai, Q.Q.; Xiao, L.R.; Pan, Z.Y.; Gao, B.; Zhou, H.; Zhu, Y.T. Dual-Phase Hetero-Structured Strategy to Improve Ductility of a Low Carbon Martensitic Steel. *Mater. Sci. Eng. A* **2022**, *834*, 142584. [CrossRef]

34. Karmakar, A.; Ghosh, M.; Chakrabarti, D. Cold-Rolling and Inter-Critical Annealing of Low-Carbon Steel: Effect of Initial Microstructure and Heating-Rate. *Mater. Sci. Eng. A* **2013**, *564*, 389–399. [CrossRef]

35. Sun, M.Y.; Wang, Z.Q.; Wang, X.M.; Shang, C.J.; Misra, R.D.K. The Significant Effect of Non-Recrystallization Zone Reduction on Microstructure and Mechanical Properties in Multi-Phase Steel from the Perspective of Crystallographic Structure and Variant Pairing. *Mater. Sci. Eng. A* **2020**, *778*, 139078. [CrossRef]

36. Sun, Y.; Li, X.; Yu, X.; Ge, D.; Chen, J.; Chen, J. Fracture Morphologies of Advanced High Strength Steel During Deformation. *Acta Metall. Sin. Engl. Lett.* **2014**, *27*, 101–106. [CrossRef]

37. Heibel, S.; Dettinger, T.; Nester, W.; Clausmeyer, T.; Tekkaya, A.E. Damage Mechanisms and Mechanical Properties of High-Strength Multiphase Steels. *Materials* **2018**, *11*, 761. [CrossRef] [PubMed]
38. Yoon, J.I.; Jung, J.; Joo, S.-H.; Song, T.J.; Chin, K.-G.; Seo, M.H.; Kim, S.-J.; Lee, S.; Kim, H.S. Correlation between Fracture Toughness and Stretch-Flangeability of Advanced High Strength Steels. *Mater. Lett.* **2016**, *180*, 322–326. [CrossRef]
39. Calcagnotto, M.; Adachi, Y.; Ponge, D.; Raabe, D. Deformation and Fracture Mechanisms in Fine- and Ultrafine-Grained Ferrite/Martensite Dual-Phase Steels and the Effect of Aging. *Acta Mater.* **2011**, *59*, 658–670. [CrossRef]